# WEATHER REGIMES ASSOCIATED WITH SUMMER RAINFALL VARIABILITY OVER SOUTHERN MEXICO

***Yanet Díaz Esteban, Graciela B. De Raga***

Universidad Nacional Autónona de México, Avenida Universidad No. 3000 CP: 04510 Ciudad de México, México, e-mail: yanet.diaz.esteban@gmail.com

## Abstract

This study focuses on the identification of weather regimes (WRs) over Mexico, the tropical eastern Pacific, Central America and the Caribbean, associated with seasonal precipitation over southern Mexico. A self-organizing maps (SOM) analysis of sea level pressure, 850-hPa horizontal winds and 925-hPa-specific humidity for the period 1997–2013 was carried out to identify the circulation patterns. This approach allowed the discrimination of wet and dry regimes, with clear and distinct features. Weather patterns exhibiting negative (positive) mean sea level pressure anomalies, southerly (northerly) winds, above- (below-) average low-level moisture and little (large) influence of the North Atlantic Subtropical High (NASH), resulted in above- (below-) average precipitation over southern Mexico. The intra-seasonal variability of the WRs and their associated rainfall is well captured by this methodology. In particular, the mid-summer drought (MSD) during late July and early August, is clearly represented by a group of patterns, which evidence a strong influence of the NASH, strong easterly winds in the Caribbean Basin and reduced low-level humidity, all factors that combine to induce below-normal rainfall over southern Mexico. The analysis of the inter-annual variability of the WRs suggests that year-to-year variations in their frequencies can impact summer rainfall in the regions of southern Mexico considered in this study. In particular, the analysis indicates that the dominant WR associated with the MSD exhibits a 3- to 4-year modulation in its frequency of occurrence, which has not been previously reported in the literature. The main MSD pattern is more frequent during dry years and has a significant correlation with the Multivariate El Niño-Southern Oscillation (ENSO) Index (MEI), indicating that MSD is stronger during 'El Niño' years. Also, WRs associated with negative (positive) rainfall anomalies showed positive (negative) correlations with the MEI, suggesting a possible modulation by ENSO phases.

## 1. Introduction

The study of rainfall variability over Mexico is of crucial relevance, given its importance for agriculture (Liverman, 1990; Conde et al., 1998, 2006), hydroelectric power generation (Blackshear et al., 2011) and overall human livelihood. Therefore, many studies have focused on rainfall variability over Mexico (García, 1965; Magaña et al., 1999, 2003; Englehart and Douglas, 2001, Cavazos et al., 2002; Magaña and Caetano, 2005; Romero-Centeno et al., 2007; Vázquez-Aguirre, 2007; Liebmann et al., 2008; Englehart and Douglas, 2010; Méndez and Magaña, 2010; Mendoza et al., 2014). A large variety of climates is observed in Mexico, from the dry deserts in the north to the tropical forests in the mountainous southern regions, which have different time scales of variability. The northwest region experiences only a concentrated, 2-month long period of rains in July and August, known as the North American monsoon (Higgins et al., 1999). In contrast, vast regions of southern Mexico experience rainfall from May to October (Liebmann et al., 2008). The distribution of precipitation is observed to be unimodal in most of central and western Mexico, while regions in thesouth and southeast experience a small reduction in rainfall during the summer (typically July–August), known as the mid-summer drought (MSD, Magaña et al., 1999), present also in Central America (Karnauskas et al., 2013). According to Curtis (2013), the extent of the warm pools present in the Caribbean Sea and eastern Pacific Ocean plays a role in the modulation of rainfall amount over the region, and there is a small contribution by sea surface temperatures (SSTs) in the El Niño (EN) 3.4 region to the inter-annual variability of the mid-summer precipitation.

The variability of the climate can be analysed through the classification of atmospheric conditions into a number of different representative states, by means of evaluating their frequency changes (Deligiorgi et al., 2014). These 'states' are defined by recurrent and persistent atmospheric circulations (Polo et al., 2011), corresponding to different weather regimes (WRs) or patterns. WRs determined from daily data may contain information of climate variability at different spatial and temporal scales and their analysis provides insight into the variability of the local climate, e.g. temperature and precipitation. Several authors (Cavazos, 1999, 2000; Nishiyama et al., 2007; Polo et al., 2011) have documented the advantages of using WRs to understand and characterize statistical and physical properties of meteorological phenomena, such as precipitation at local scale.

There are a number of statistical methods that allow the identification of WRs. One of the most effective tools is an artificial neural network called self-organizing maps (SOM), a non-linear classification technique developed by Kohonen (1982). It is based on unsupervised and competitive learning and allows the projection of high-dimensional data into a two-dimensional map. SOM have been recently used within the field of atmospheric sciences to study a range of phenomena, given that it is a powerful tool for visualization of spatially organized sets of patterns. This methodology has been used for general circulation models evaluation (Cassano et al., 2006; Hope, 2006; Finnis et al., 2009a, 2009b; Skific et al., 2009a, 2009b; Steynor et al., 2009); for teleconnection studies and evolution of the monsoon systems (Cavazos et al., 2002; Reusch et al., 2007; Chattopadhyay et al., 2008; Johnson et al., 2008; Tozuka et al., 2008; Johnson and Feldstein, 2010; Guèye et al., 2011; Bao and Wallace, 2015) and for examination of the relationship between atmospheric circulation and rainfall (Cavazos, 1999, 2000; Hewitson and Crane, 2002; Tennant and Hewitson, 2002; Gutiérrez et al., 2005; Nishiyama et al., 2007; Alexander et al., 2010; MacKellar et al., 2010; Tymvios et al., 2010; Polo et al., 2011; Espinoza et al., 2012; Chattopadhyay et al., 2013; Oettli et al., 2014; Ohba et al., 2015). All these studies extracted climate modes or weather patterns from multidimensional, non-linear input data (i.e. with a complex statistical relationship between them) using SOM analysis.

In this study, we apply the SOM approach to investigate the relationships between synoptic weather types and anomalous precipitation during the rainy season over two regions of interest in southern Mexico. Furthermore, we investigate the variability of WRs at different time scales as well as the influence of large-scale systems on WR frequency. Two regions have been selected for this study: the Balsas River basin (17.0° –20.0°N; 103.5° –97.0° W) and the Yucatan Peninsula (17.5° –21.6° N; 93.9° –86.6°W) (Figure 1). Both regions are located in the southern part of Mexico and have large uniformity in their characteristics (a river basin and a plain, respectively), which makes them not only separate geographic areas but distinct climatic regions. Figure 1 shows the topography for both regions. At the northern side of the Balsas River basin there are mountains with elevations above 5000 m, corresponding to the 'Eje Volcánico Transversal'. The 'Sierra Madre del Sur' mountain (up to 3500 m above sea level) limits the basin to the south. In contrast, the Yucatan Peninsula shows a plain topography, with elevations below 200 m above sea level.

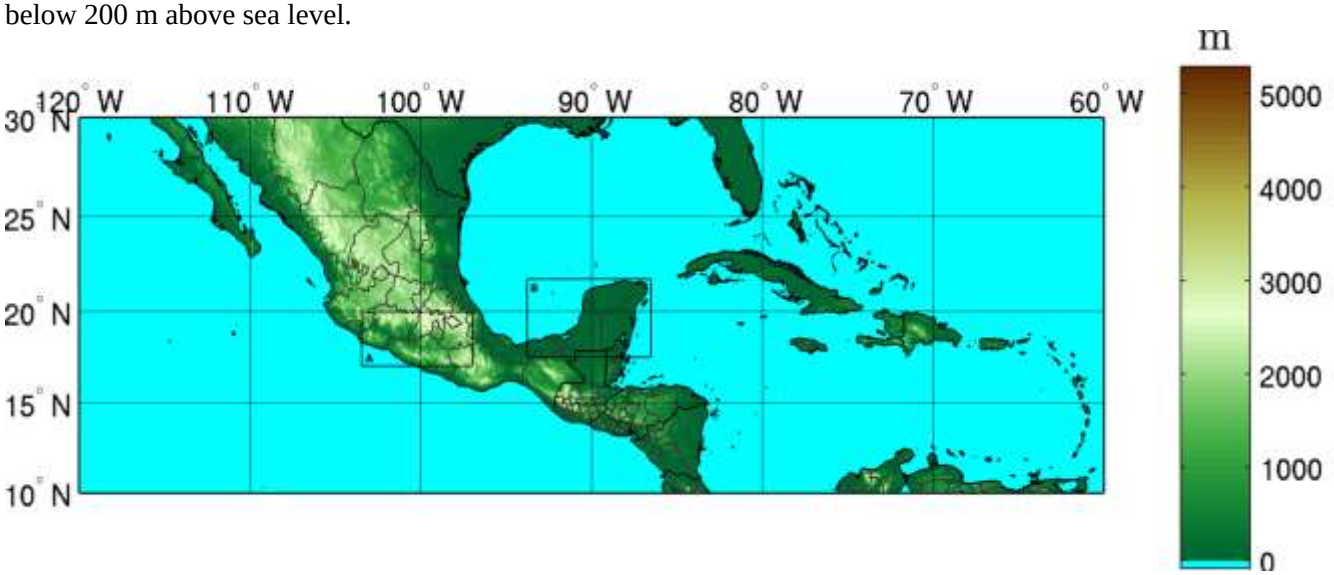


Figure 1. Study area with topography. Boxes A and B indicate subregions of study: Balsas River basin and Yucatan

Peninsula, respectively.

## 2. Materials and Methods

### 2.1 Self-organizing maps

SOM is an artificial neural network employed for cluster analysis, which provides a spatially ordered set of variability patterns when applied to atmospheric data. These patterns captured from SOM present continuity in the data space due to conservation of the topology of the structure (Polo et al., 2011), which allows the identification of large-scale atmospheric regimes. Johnson and Feldstein (2010) showed that the Northern Hemisphere intraseasonal to inter-decadal atmospheric variability can be understood in terms of changes in the frequency distribution of the cluster patterns that comprise this continuum. Therefore, this neural network model is robust for the analysis of regional climate variability and, in particular, for investigating weather patterns associated with anomalous precipitation.

The algorithm is based on a grid of neurons (or nodes) with an associated weight vector m = [m1 , m2, ...., md] with the same dimension as the input data x. A detailed description of the SOM method can be found in many papers, such as in Vesanto and Alhoniemi (2000), Kohonen (2001) and Elghazel and Benabdeslem (2014). In the present work, the batch training algorithm has been employed, which is fast and computationally more economic than other implementations of the SOM. As an outcome of this algorithm, the neurons on the grid become ordered in the sense that nearby neurons have closer weight vectors (Vesanto et al., 2000). The four corners of the matrix of SOM can thus be thought of as the most extreme nodes in terms of climate variability, with a smooth continuum in between (Sheridan and Lee, 2011).

We selected a 16-node SOM grid (a 4 × 4 rectangular grid), after testing other sizes of the SOM grid (or Kohonen map) and determining that a 4 × 4 array represents a suitable balance between computational cost and representativeness of synoptic patterns. After a review of the literature, a rectangular lattice of the array and a pseudo-Gaussian neighborhood function were selected as parameters for the algorithm, after also performing several experiments varying those parameters.

### 2.2 Data and study area

A large area centred over southern Mexico (10.0° –30.0° N; 120.0° –60.0°W) was selected to evaluate the variability of WRs that affect precipitation over Mexico, as shown in Figure 1. This area comprises not only Mexico but also the Tropical Eastern Pacific, Gulf of Mexico, Caribbean Sea and part of the tropical North Atlantic ocean, given the modulation on precipitation exerted by these oceanic regions (Méndez and Magaña, 2010; Curtis, 2013). The subregions indicated by the two black boxes in Figure 1 correspond to the basin of the Balsas River and the Yucatan Peninsula.

The European Centre for Medium-Range Weather Forecast (ECMWF) reanalysis ERA-Interim provides the atmospheric information for the cluster analysis. Daily data at a moderately high-resolution version of the reanal ysis (0.5° × 0.5°) on a regular grid are employed. The following variables were selected for the analysis: mean sea level pressure (MSLP), specific humidity at 925-hPa pressure level (q925) and 850-hPa zonal and meridional wind components (u850, v850). Although not used in the algorithm, the vertical velocity at 600-hPa level was also employed for the analysis because of its associations with humidity and cloud fields. The rainfall is estimated from the Climate Hazards Group InfraRed Precipitation with Station (CHIRPS) data set, which incorporates 0.05° resolution satellite imagery with in situ station data to create gridded rainfall time series for trend analysis and seasonal drought monitoring (Funk et al., 2015).

The period selected for the analysis covers 1997–2013 (17 years). This particular period enables the comparison between rainfall patterns obtained from CHIRPS and Global Precipitation Climatology Project (GPCP) (Huffman and Bolvin, 2013) data sets, since the latter is available only from October 1996.

To investigate summer precipitation, only the period between 1 May and 31 October of each of the 17 years is used. Anomalies are computed by subtracting the long-term mean for the period 1997–2013 to daily values.

Furthermore, anomalies are normalized to ensure that all the meteorological fields account for the same weight in the analysis and weighted by the cosine of latitude to account for the dependence of the grid-point density on latitude. Variables are arranged on a matrix (days × grid points) (Equation (1), so that every daily vector contains information on surface pressure, low level tropospheric moisture and circulation, thus incorporating into the algorithm both thermodynamic and dynamic variables.

$$X(d\times p) = MSLP(d\times p), q925(d\times p), u850(d\times p), v850(d\times p) \quad (1)$$

where d = 3128 days and p = 4961 grid points. As a result, the SOM algorithm generates a non-linear classification of these multivariate daily data into 16 categories or climate modes. After the SOM analysis is performed, the daily fields of several meteorological parameters are classified into one of the 16 modes. Then,
composite maps of daily anomalies for each weather pattern are computed.

## 3. Results

### 3.1 WRs: general features

The long-term seasonal means (from May to October) of sea level pressure, 925-hPa-specific humidity and 850-hPa wind are displayed on Figure 2. The North Atlantic Subtropical High (NASH) of the Azores-Bermuda is evident, spreading its influence through most of the Caribbean Basin with a wind circulation mostly from the east, showing the strongest winds south of 20∘ N and east of 95∘ W. The 16 WRs identified by the SOM analysis (Figure 3), are presented in terms of MSLP and 850-hPa wind, as anomaly composites with respect to the long-term seasonal means shown in Figure 2.

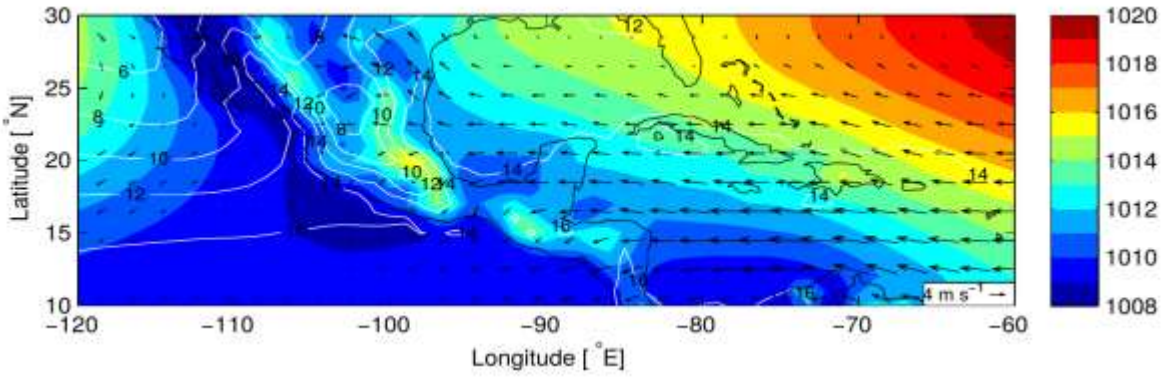


Figure 2. Long-term average (1997–2013) of the MSLP (colour scale, in hPa), 925-hPa-specific humidity (contour lines, in g/kg) and 850-hPa wind (vectors, in m/s) for MJJASO, from ERA-Interim.

As previously mentioned, the SOM algorithm ensures that closer or adjacent modes in the matrix are more closely related than those that are distant, due to the inherent characteristic of the algorithm of preserving the topology of the input data. Another consequence of this feature of the SOM is that modes on opposite corners represent extremely different patterns, while the intermediate patterns are possible transition states between extremely different regimes, as was also reported in other studies using the SOM methodology (e.g. Cavazos et al. 2002; MacKellar et al. 2010; Polo et al. 2011; Henderson et al. 2017). Note that in Figure 3 the patterns in which high-pressure anomalies are dominant are aligned on the left side of the matrix, while patterns with dominant low-pressure anomalies appear on the right side of the matrix. The preservation of the topology of the input data represents a remarkable advantage over other clustering methods, because it enables an easier interpretation of the results and allows the detection of possible transitions between regimes, which could be important for seasonal prediction. The month when each of the modes is more likely to occur (indicated at the top of each map) provides insight into the intra-seasonal variability of the WRs. For example, WRs 1,4 and 4,1 which represent opposite MSLP and winds anomaly patterns, characterize the end of the season (October), indicating the alternation of the atmosphere between lower and higher than average surface pressure above eastern Mexico and the gulf in this time of the year. Furthermore, WRs 1,1 and 4,4 which also evidence opposite MSLP and winds patterns in terms of the anomalies, are more frequent at the beginning of the season (May).

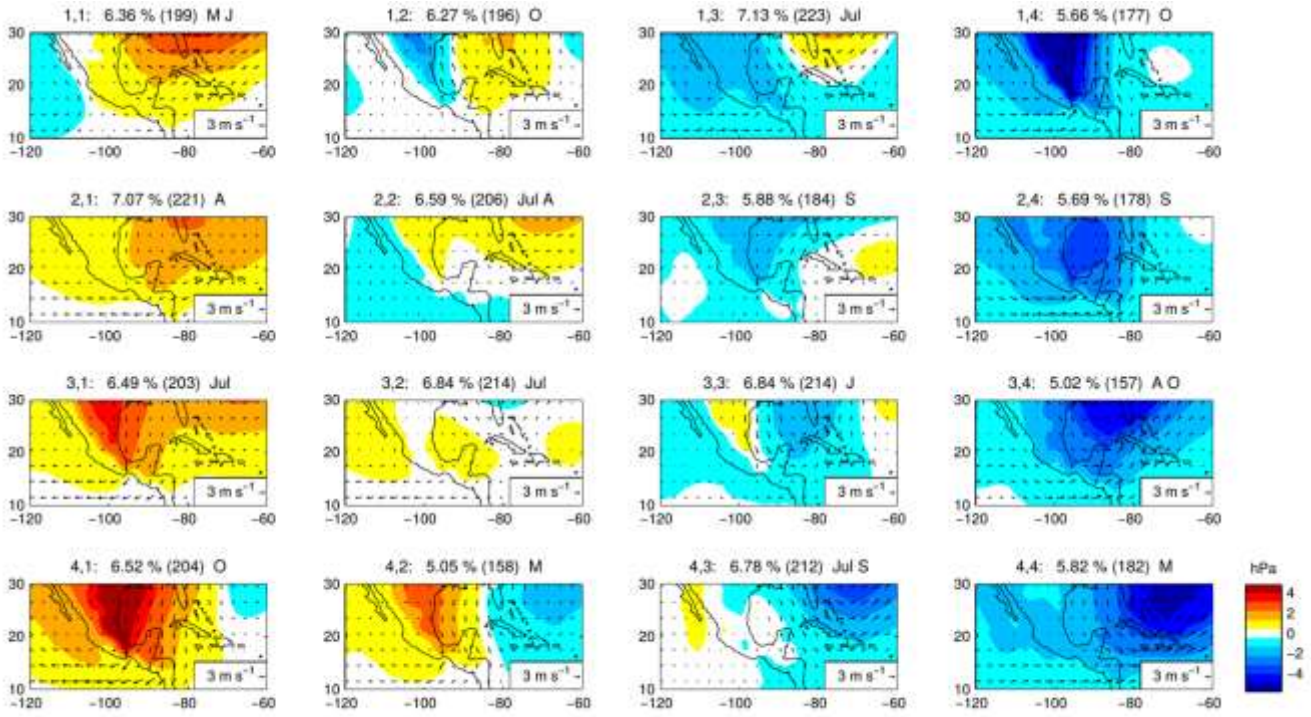


Figure 3. MJJASO WRs in terms of the anomalies of the mean the sea level pressure (colour scale, in hPa) and 850-hPa wind (vectors, in m/s) for the period 1997–2013. The WR were obtained from the SOM analysis from MSLP, 925-hPa-specific humidity and 850-hPa zonal and meridional wind. The position (i, j) of each WR in the matrix, relative frequency (in %), total number of days and the months of more likely occurrence for each WR are indicated at the top of each map.

This represents the oscillation on intensity and location of the NASH around this month, when the rains of the wet season start. Note that WRs at the centre-left of the SOM matrix, (labelled as 2,1; 2,2; 3,1 and 3,2) occur more frequently in the middle of the season (July and August), coinciding with a decrease of the rainfall amounts expe rienced in southern Mexico. Those modes show patterns with positive MSLP anomaly over most of Mexico and the western Atlantic (slightly less noticeable in WR 3,2). Furthermore, WRs 1,2 and 4,2 have opposite anomaly dipole patterns: WR 4,2 indicates positive MSLP anomalies over Mexico and the Gulf and negative anomalies over the Atlantic, and is more likely to occur in May, while WR 1,2 shows negative MSLP anomalies over Mexico and western Gulf of Mexico and positive anomalies over the western Atlantic, northern Caribbean and eastern gulf, and is more likely to occur in October.

The detailed evolution of the frequency distribution of each of the WRs throughout the season, between May and October, is shown in Figure 4. Note that WRs 2,1 and 2,2 exhibit a high frequency of occurrence in late July and August and that WR 3,2 has its maximum frequency also in July, but at the beginning of the month. The onset of the rainy season (in May) is characterized by a most frequent occurrence of WRs 1,1 and 4,4 while WRs 1,4 and 4,1 are more frequent at the end of the rainy season.

To further explore the synoptic-scale variability of the WRs, an event was defined as a sequence of consecutive days with the same dominant WR lasting a minimum of 2 days. The number of such events and the mean persistence of each one of them are shown in Figure 5. Note that WRs identified as 2,1; 1,3; 3,1 and 4,1 present the highest number of events; however, the persistence of these events is not high. Instead, the largest average persistence is seen for WRs 4,4 and 4,1 (more than 3 days), followed by WRs 1,1 and 2,4 (more than 2.8 days). This is important because changes in the persistence or number of events of a particular WR could account for the probability of occurrence of a phenomenon, such as more precipitation in a given area (Polo et al., 2011).

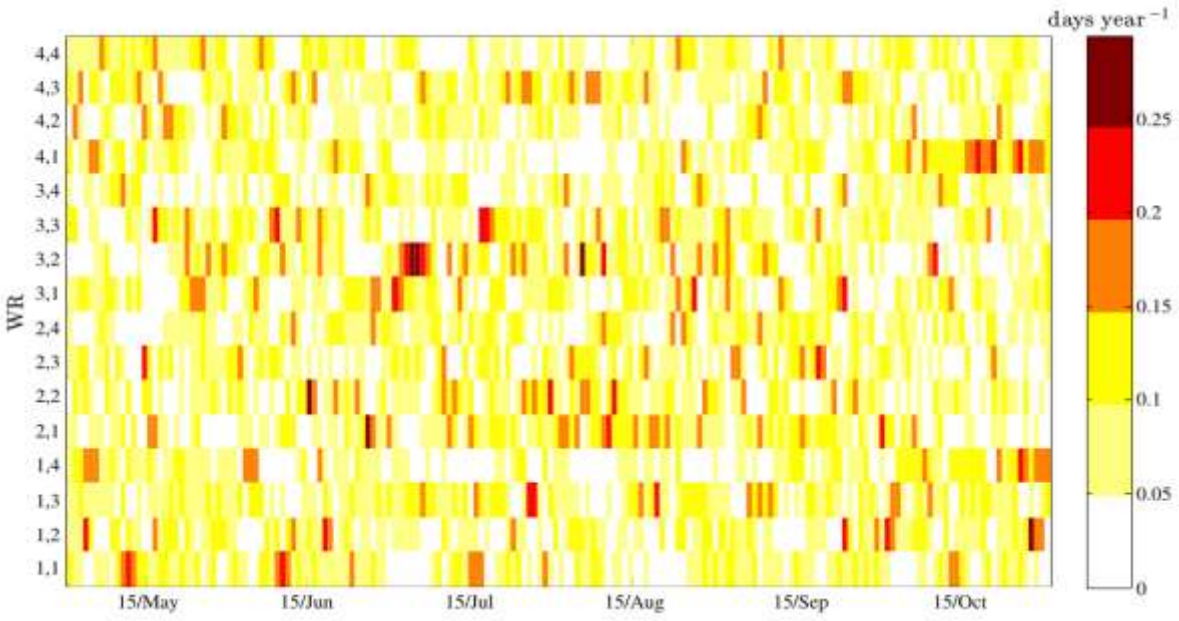


Figure 4. Intra-seasonal evolution of the mean frequency of each WR.

3.2. Rainfall and WRs in southern Mexico

3.2.1. Long-term mean precipitation

Composites of daily data from CHIRPS were computed in order to study the precipitation associated with each WR, based on the long-term seasonal mean from May to October (Figure 6). The average rainfall is mostly uniform over the Yucatan Peninsula, with values between 2 and 3 mm/day, while the Balsas River basin presents higher spatial variability, associated with a more complex topography. Note that the largest accumulation within the Balsas River basin is observed in the southern parts and the Pacific coast of the subregion, with values ranging between 8 and 12 mm/day . The monthly climatology over 1997–2013
for the two regions is shown in the top row of Figure 7, for the Balsas River basin (left) and the Yucatan Peninsula (right). While the monthly mean values are similar in magnitude in both regions, note that there is a somewhat different seasonal cycle in each region. In particular, the month of July in the Yucatan shows an intra-summer relative minimum (evidence of the MSD). The MSD is a feature of the annual cycle of precipitation observed in southern Mexico and Central America, where rainfall amounts are reduced by roughly 40% in late July and early August compared to June and September (Magaña et al., 1999). The rainiest month in both regions is September. The frequency distributions of precipitation (Figure 7, bottom row) are bimodal in both regions; however, the most frequent daily value is 1 mm/day in the Balsas River basin (left panel) while 2- to 3-mm/day rainfall is more frequent in Yucatan. Both regions also show a more frequent intense daily precipitation between 7 and 8 mm/day , with 7 mm/day more frequently observed over Yucatan. The secondary peak observed in both regions could be rainfall linked to certain synoptic scale systems, such as tropical cyclones.

3.2.2. Rainfall anomalies related to WRs

The composite anomalies of daily rainfall associated with each WR are displayed in Figure 8. It is clear how the WRs identified in the previous section are associated with different spatial distributions of precipitation anomalies. For example, note that WRs on the lower left corner of the SOM matrix (2,1; 2,2; 3,1; 3,2; 4,1; 4,2; 4,3) induce strong negative rainfall anomalies in the Balsas River basin. Maximum negative rainfall anomalies up to −8 mm/day are seen for WR 4,1, corresponding to the most extreme among all WRs with negative anomalies and most frequently observed in October. In contrast, the four WRs on the upper right corner of the SOM matrix (1,3; 1,4; 2,3 and 2,4) all lead to positive rainfall anomalies over that same river basin.

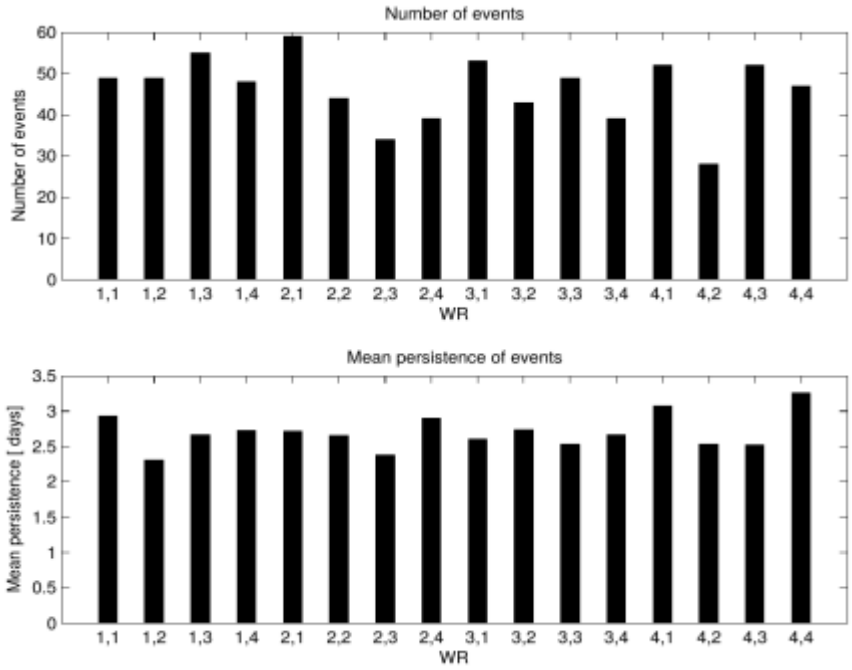


Figure 5. Number of events (top panel) and mean persistence (bottom panel) of each WR.

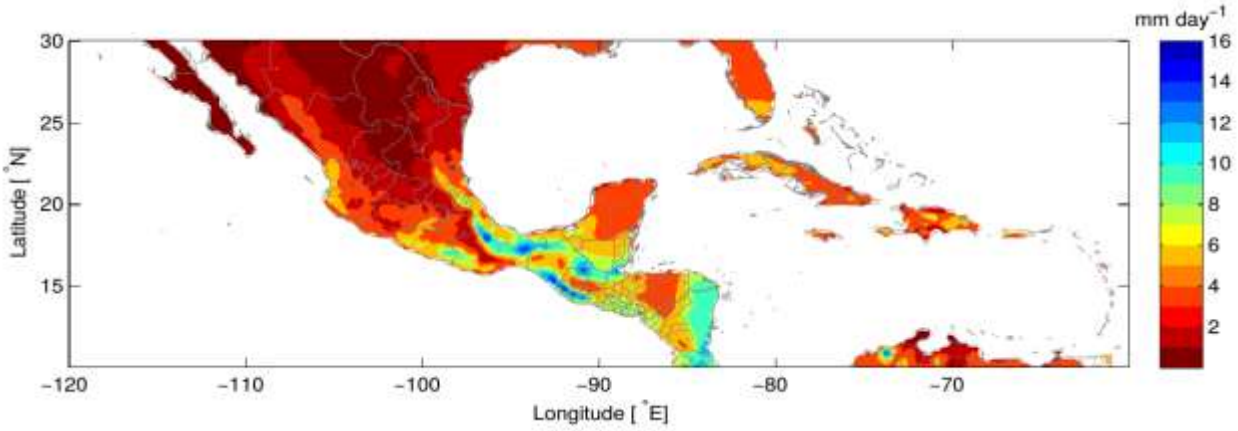


Figure 6. Long-term seasonal (MJJASO) mean daily rainfall for the period 1997–2013, in mm/day , from CHIRPS.

A slightly different relationship between WRs and precipitation anomalies is observed for the Yucatan Peninsula. The largest negative rainfall anomalies (with values up to −4 mm/day) are associated with WRs 1,2 and 1,4, both occurring more frequently in October. WRs at the lower left corner of the SOM matrix and indeed the whole bottom row are associated with negative rainfall anomalies over Yucatan. The exception is seen for WR 3,1, which is associated with a positive anomaly more likely to occur in early July. Some of the WRs in the upper right corner of the matrix, such as 1,3; 2,4 and 2,3 (only for the north of the peninsula) are related to positive rainfall anomalies. These WRs induce similar responses in precipitation anomalies in both the Balsas River basin and the Yucatan Peninsula.

These differences in the precipitation anomalies in the two subregions studied here suggest that the same WRs are inducing diverse responses. To better understand these differences, composites of selected meteorological variables for each WR were also computed. Composites of the specific humidity at 925-hPa and 850-hPa winds are displayed in Figure 9. Low-level moisture over southern Mexico is higher on WRs located in the upper right corner of the SOM matrix, specifically WRs 1,3; 1,4; 2,3; 2,4, reaching values up to 16 g/kg, which corresponds to about 2 g/kg greater than typical values for the region. Moreover, those WRs are associated with southerly winds at 850 hPa in both subregions, bringing moisture from the Caribbean to the Yucatan Peninsula, and from the Pacific

Ocean to the Balsas River basin. It is noteworthy that for WR 1,4, the wind speed is high over the entire region of Yucatan, with values up to 10 m/s, corresponding to the largest magnitudes compared to all other WRs. These high wind speeds are produced by a strong surface pressure gradient between the NASH and a thermal depression over the Mexican Plateau for this WR (1,4 in Figure 10).

Such strong low-level winds could also be causing the subsidence observed over this region in Figure 11 for this WR, and thus explain the strong negative rainfall anomalies over Yucatan. The WRs in the upper corner of the SOM grid are similar to the East North Atlantic High (ENAH) pattern in Sáenz and Durán-Quesada (2015), who also found an eastward displaced NASH, low pressures over Mexico and the Gulf of Mexico and anticyclonic flow over the tropical Atlantic–Caribbean sector for this regime.

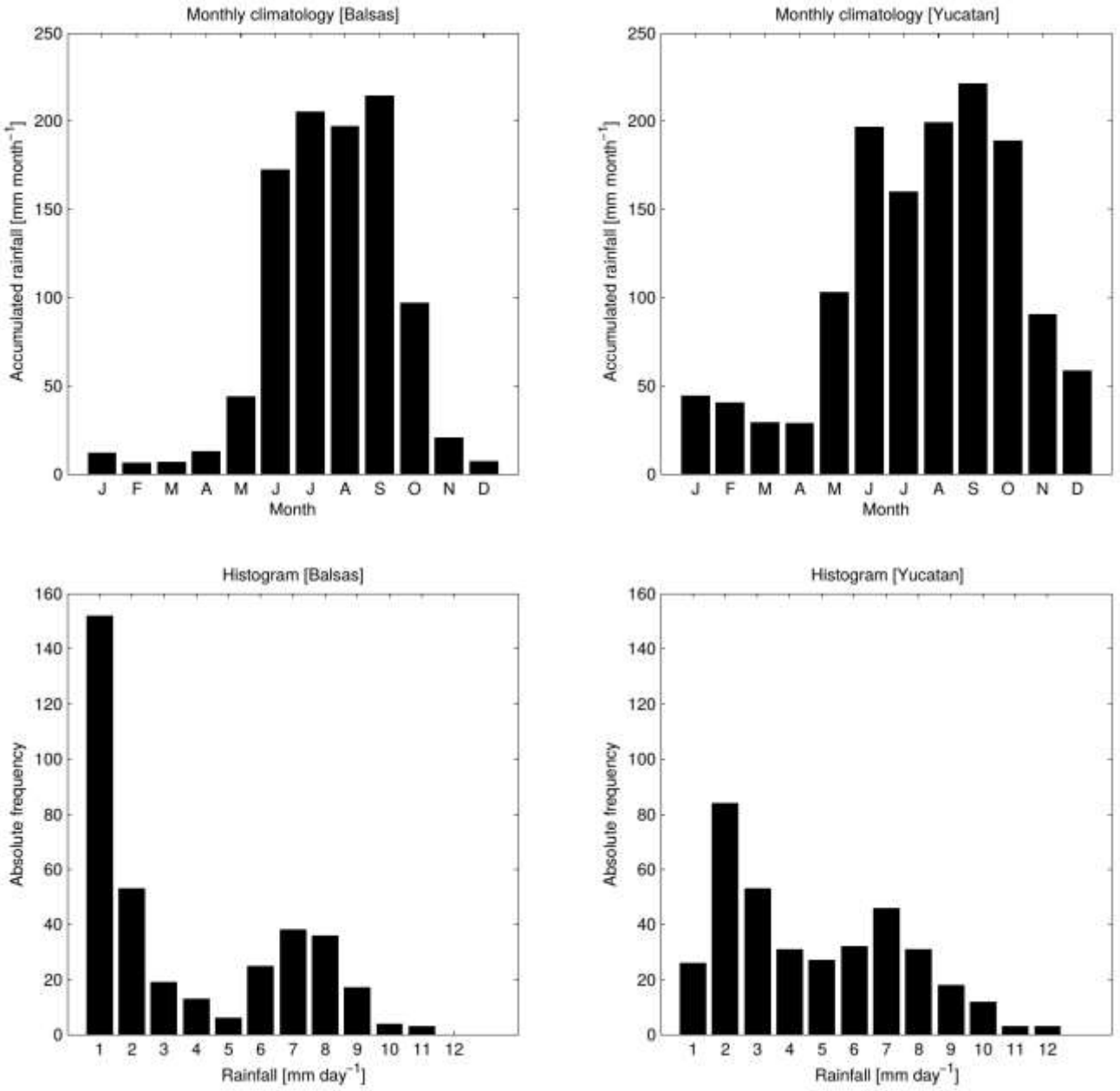


Figure 7. Monthly climatology of accumulated rainfall (top panels) and frequency distributions of daily precipitation (bottom panels) for the Balsas River basin (left column) and the Yucatan Peninsula (right column).

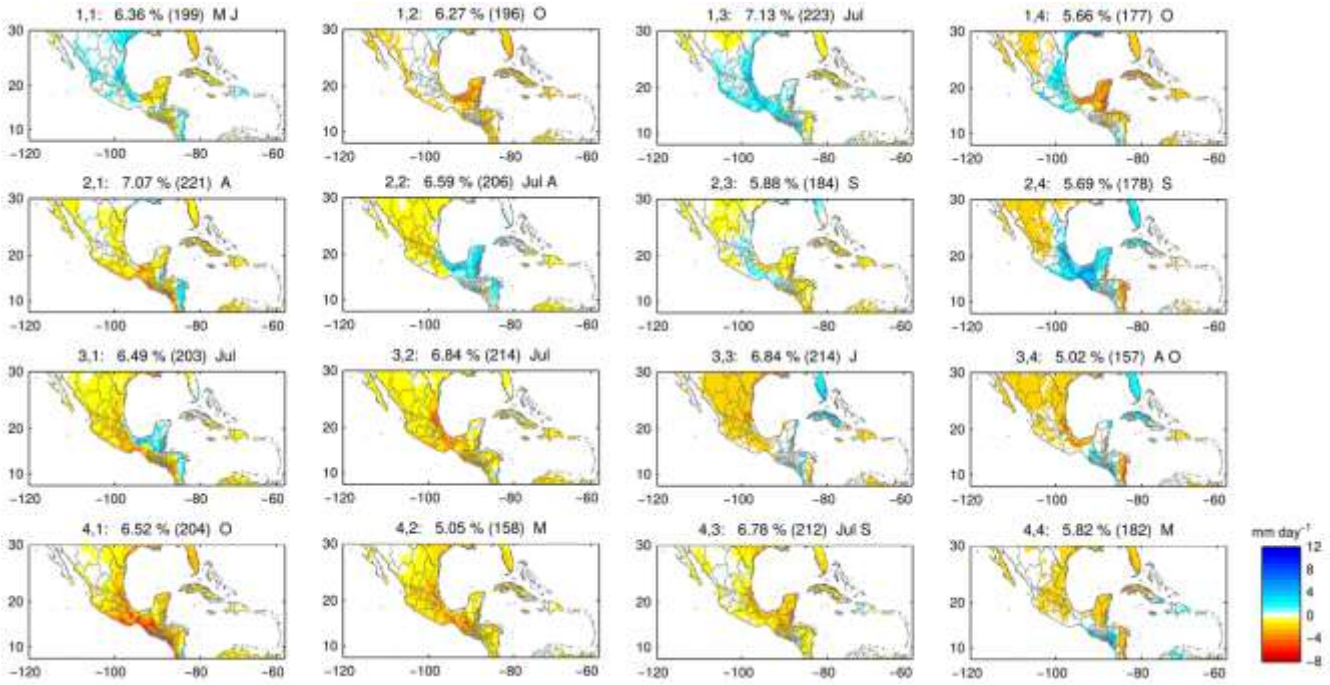


Figure 8. Anomaly composites of daily precipitation for each WR, in mm/day , from CHIRPS. The statistical significance of the precipitation field is shown in Figure S4.

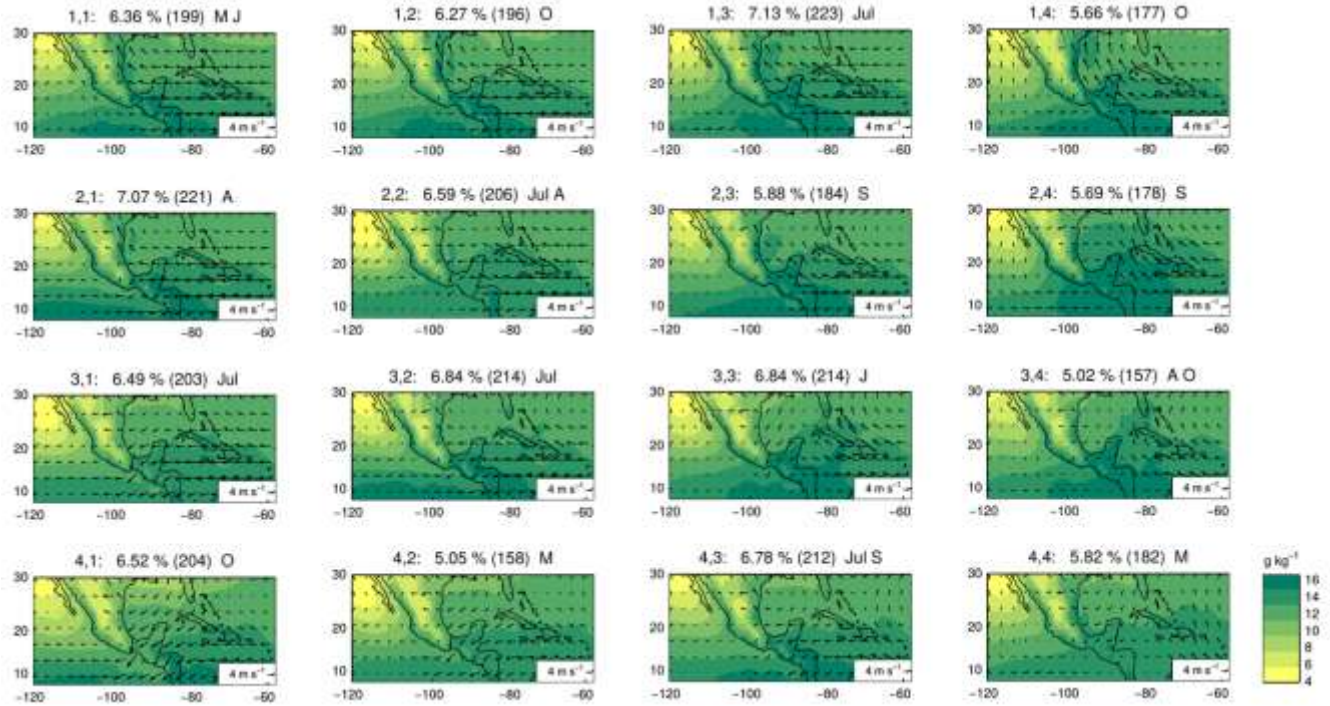


Figure 9. Composites of daily specific humidity at 925-hPa (shaded areas, in g/kg ) and 850-hPa winds (vectors, in m/s) for each WR, from ERA-Interim.

WRs at the centre left of the SOM grid (2,1; 2,2; 3,1; 3,2) show evidence of strong low-level winds in the southern Caribbean Sea (Figure 9), with values up to 14 m/s , a pattern that clearly resembles the Caribbean Low Level Jet (CLLJ). The CLLJ is a maximum of the easterly zonal wind (stronger than 13 m/s) observed in the lower troposphere of the Caribbean (near 925 hPa) during the summer (Amador, 1998). It can be understood as an extension of the trade wind regime amplified by regional gradients in MSLP and temperature. Those WRs are more likely to occur in July and early August (as observed in Figure 4), coinciding with the period when the CLLJ

has a maximum during boreal summer. The composite maps of MSLP for each WR (Figure 10) indicate that Wrs 2,1; 2,2; 3,1; 3,2 show the NASH extending westward and covering the eastern part of Gulf of Mexico and the Greater Antilles, which agrees with other authors who have found this pattern of MSLP over the North Atlantic in late July and early August (Romero-Centeno et al., 2007; Wang, 2007). Those WRs resemble one of the patterns that Sáenz and Durán-Quesada (2015) found for the summer, in particular, the Summer Low Level Jet (SLLJ in their study). Those regimes could also be representative of the MSD, a feature of the annual cycle of precipitation in southern Mexico and Central America (Magaña et al., 1999). Daily rainfall anomalies (Figure 8) show negative values over the Balsas River basin for WRs 2,1; 2,2; 3,1; 3,2 with values up to −6 mm, that could be related to an intensification of the flow over the Tehuantepec Isthmus referred to as 'Tehuantepec Jet', as documented by Romero-Centeno et al. (2007). For the Yucatan region, the same behaviour is observed except for WR 2,2 and 3,1, which evidence positive anomalies. The above-normal precipitation for WRs 2,2 and 3,1 may be associated with local or thermodynamic factors, and further research is needed to explain this behaviour.
Moisture and wind patterns (Figure 9) for WR 4,1, –which evidences the strongest negative anomalies over Balsas and not as strong but still below-average values over Yucatan – show low humidity over both areas and a wind flow from the northeast, consistent with a high-pressure system centred at (30◦ N, 90◦ W), as seen in the MSLP maps (Figure 10). The 600-hPa vertical velocity composites (Figure 11) indicate subsidence over most of the Balsas River basin, while insignificant vertical motion is seen over the Yucatan Peninsula.

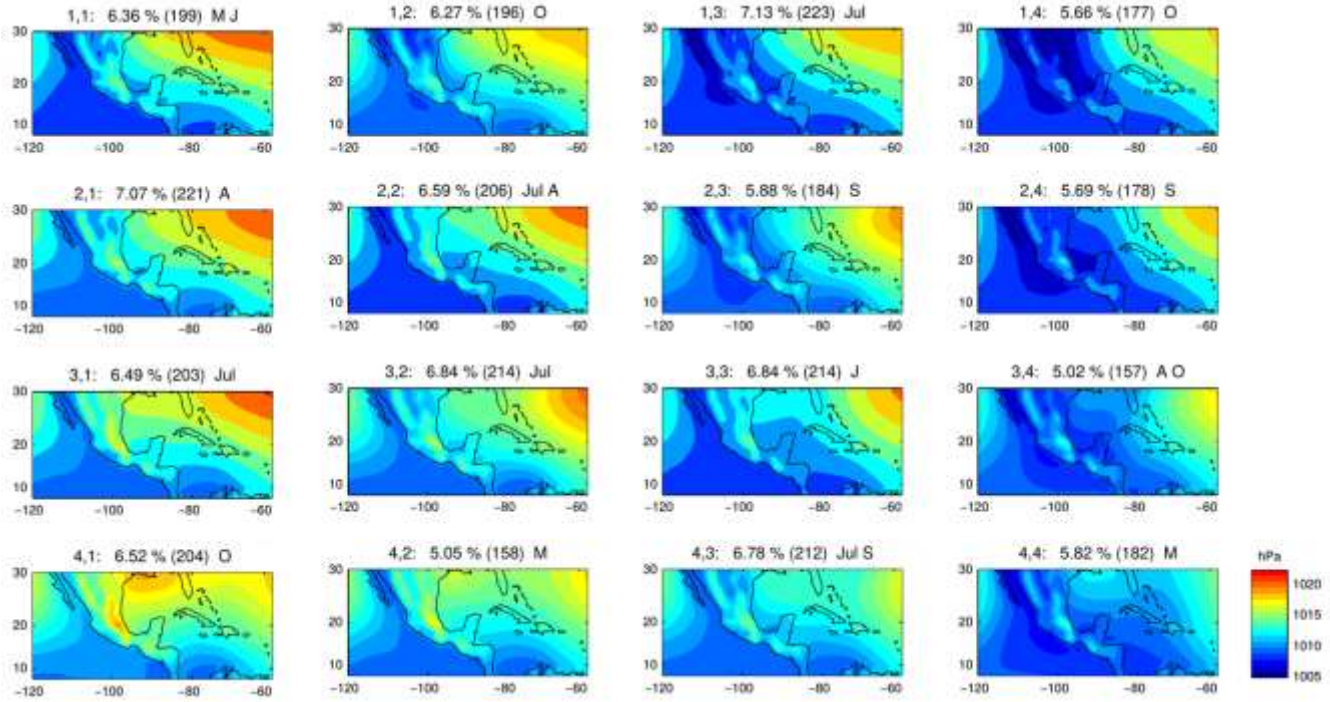


Figure 10. Composites of daily MSLP, in hPa, for each WR, from ERA-Interim.

3.3. Inter-annual variability of WRs

To study the inter-annual variations of the frequency of WRs and their associated rainfall, we first classify years as 'wet' or 'dry', based on an accumulated seasonal rainfall index, computed for each of the two subregions (Figure 12). To compute that index, area-averaged rainfall amounts during each MJJASO season of the period 1997–2013 over the Balsas River basin are calculated, and the seasonal mean of the period 1997–2013 is subtracted from every year's MJJASO amount. A similar calculation is done for the Yucatan Peninsula. Thus, anomalous values for every year on each of the two subregions are obtained. Years with index values above zero are classified as 'wet', while years with below-zero index values are classified as 'dry'.

The differences in persistence and number of events for each WR between wet and dry years were computed and are shown in Figure 13. For the Balsas subregion, WRs 1,1 to 1,4 (first row of the SOM matrix) and also WRs 2,2; 2,3 and 4,3 present a larger number of events in anomalously wet years, while the rest of the WRs have more events in anomalously dry years. However, for the Yucatan subregion, the higher occurrence of WR events

of the right column of SOM matrix (1,3; 1,4; 2,4; 3,4; 4,4) is more evident in wet years, while the rest of the WR have more events in dry years or do not experience changes in the frequency of their events from one year to another. It is noteworthy that the majority of WRs over the Yucatan subregion have more persistent events in anomalously dry years. In general, for both subregions, the regimes showing a high-pressure anomaly centered near 27◦ N and 100◦ W, with anomalous anticyclonic circulation associated (3,1; 4,1 and 4,2) have more number of events in dry than in wet years; while the regimes exhibiting the opposite anomaly pattern (1,3; 1,4 and 2,4) have more events, in average, in wet than in dry years.

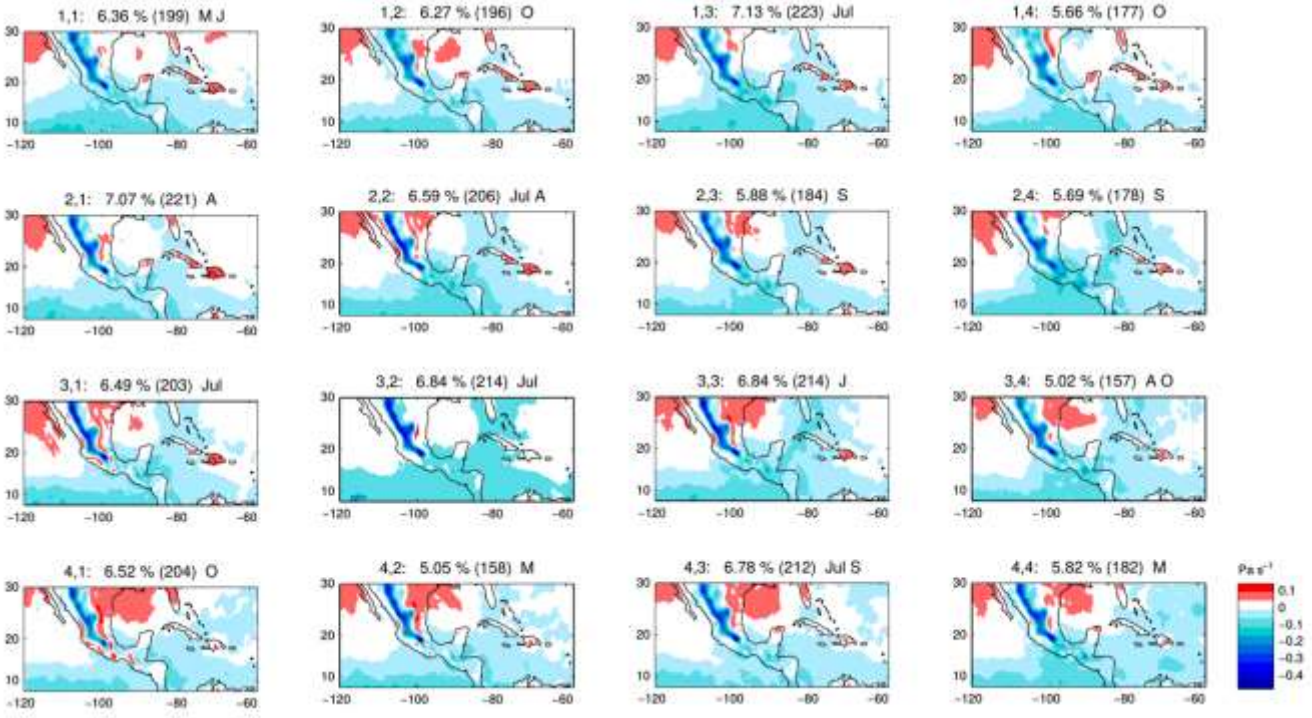


Figure 11. Composites of vertical velocity at 600-hPa level (in Pa s−1 ) for each WR, from ERA-Interim.

Figure 12.

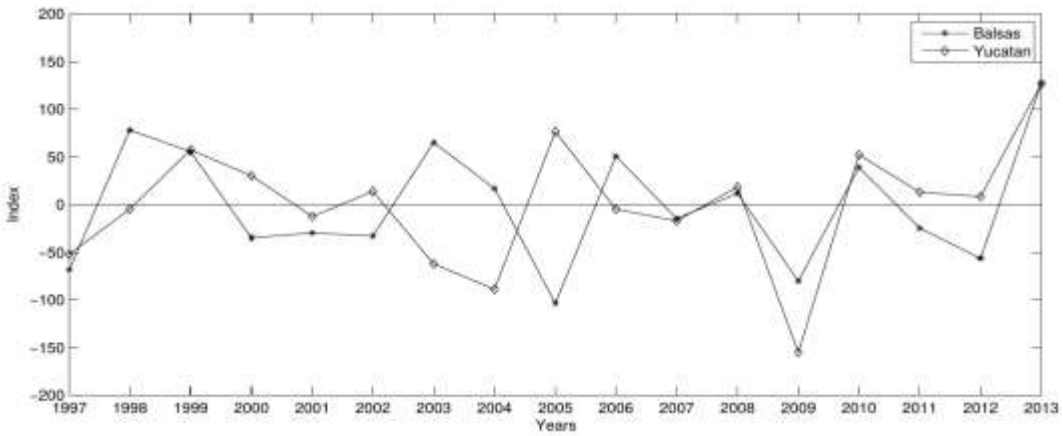


Precipitation index computed as the anomalous rainfall in every MJJASO season with respect to the mean seasonal rainfall for the period 1997–2013.

Thus, the occurrence of some WR increases when years of negative anomalous rainfall occur over southern Mexico, suggesting that year-to-year changes in the WR frequency could influence the rainfall variability at the inter-annual scale over that subregion. To further explore this idea, the absolute frequency of every WR over the entire 17-year period is presented in Figure 14. The most noticeable result is that WRs 2,1 and 2,2 – previously related to the MSD – show an increased frequency every 3–4 years, which is evidenced by the frequencies ≥15 at

years 1997, 2002–2003, 2009 and 2013. This increase in frequency results in a slight decrease in rainfall of MJJASO season over both the Balsas and Yucatan subregions for those years (Figure 14, bottom panel). In the Balsas subregion, rainfall accumulations experience an increase in years 1998, 2010, 2011 and 2013, coinciding with an increase of WRs at the top-right corner of SOM matrix (1,3; 1,4; 2,3; 2,4). As an example, during 2010 the WR 2,4 occurred often and the MSD is not evident.

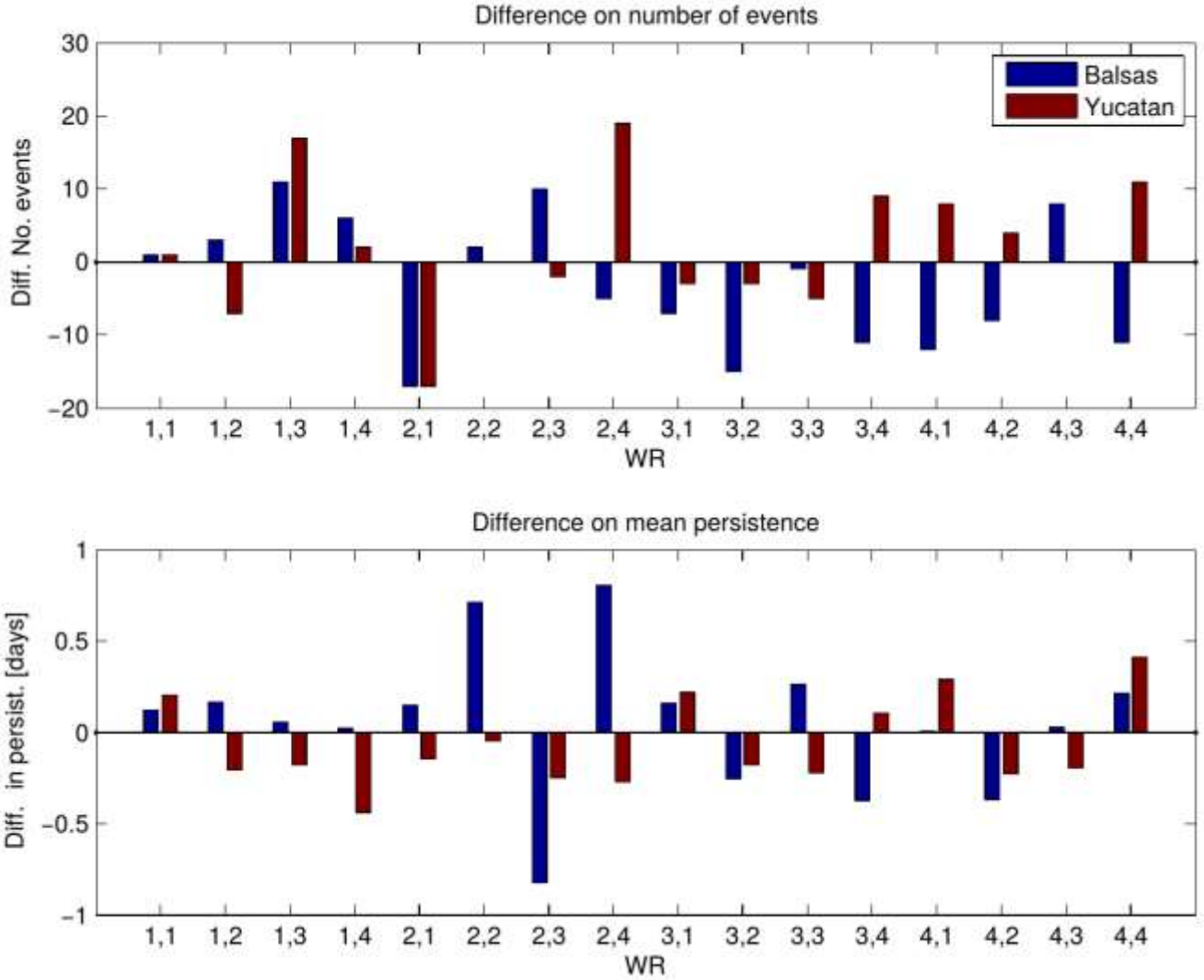


Figure 13. Difference of number of events (top panel) and persistence (bottom panel) for each WR between years of anomalous positive and negative rainfall over Balsas and Yucatan.

3.3.1. ENSO effects on the WR

To better understand the year-to-year variability of WRs – and therefore, of the summer rainfall – we assess the impact of ENSO events on the frequency of Wrs, given that ENSO is the dominant mode of inter-annual climate variability in global climate. Some authors have documented that precipitation in northern Mexico is affected by ENSO phases (Brito-Castillo et al., 2003; Magaña et al., 2003; Englehart and Douglas, 2006), nevertheless, the influence of this oscillation on precipitation in the southern part of the country is unclear. The definition of warm ('EN'), cold ('La Niña, LN') or neutral ENSO conditions within the 1997–2013 period, is based on the Multivariate ENSO Index (MEI), which is computed as the first principal component of six filtered and standardized atmospheric fields observed over the Tropical Pacific (Wolter and Timlin, 1993). The relative frequencies of the WRs during 'EN' and 'LN' years are shown in Figure 15.

A roughly opposite behaviour can be observed in the frequency of WRs according to the ENSO phase (EN vs LN

years), indicating that ENSO may modulate the probability of occurrence of each WR, and thus modify the prevalence of a particular regime during EN and LN events. EN (LN) years seem to induce the more (less) likely occurrence of the WR 2,1, a pattern of strong low-level winds in the Caribbean Basin and positive MSLP anomalies over Mexico, which result in below normal precipitation over southern Mexico. WRs 3,1; 3,2 and 3,3 are also likely to occur in EN years, inducing negative rainfall anomalies, with the exception of WR 3,1 over Yucatan. Frequencies of WRs 1,3; 1,4 and 2,4 increase (decrease) during LN (EN), which indicates that above- (below-) normal rainfall over southern Mexico is seen during the rainy season in those years. Note however, that certain WRs (1,2; 2,2; 3,3; 4,2; 4,3) do not seem to be affected by ENSO phases, as indicated by the small difference in their frequencies between EN and LN years. Indeed, linear correlations between the regime frequencies and the standardized MEI (Table 2) shows that correlations for those WR are low.

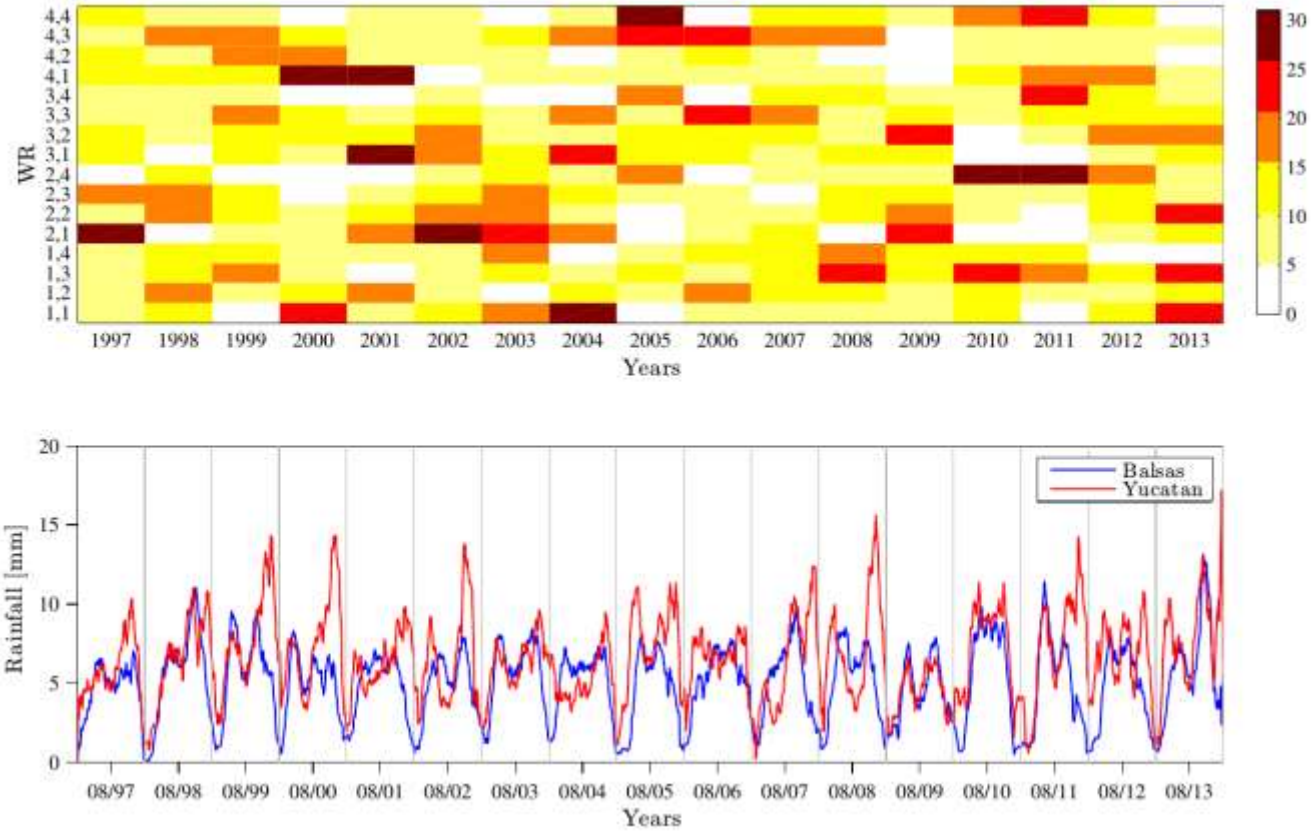


Figure 14. Frequency time series corresponding to each WR between the period 1997–2013 (top panel) and 30 days running mean of daily rainfall (area-averaged) over the period 1997–2013 (bottom panel). Only daily values from MJJASO season were used. Tick marks indicate 1 August of each year within the period 1997–2013.

Significant positive correlations are found for WRs 2,1 (0.69), 3,1 (0.58) and 3,2 (0.63), indicating an increase in the frequencies of those WR with the arrival of an EN event. This partially explains the bellow-normal rainfall amounts during summer of EN years in southern Mexico. On the other hand, one significant negative correlations exists for WR 1,3 (−0.55), suggesting that an increase in its frequency – with positive rainfall anomaly associated – is related to the occurrence of LN event.

## 4. Summary and conclusions

Understanding the variability of precipitation over Mexico is necessary given its importance for agriculture and hydropower generation. Moreover, the ability to link inter-annual variability with prevalent weather patterns could potentially contribute to improve seasonal climate predictions. The technique of SOM was used in this study and is shown to be a useful clustering tool to provide a reliable representation of WRs in a given area, and useful information on the links between large-scale weather patterns and daily surface precipitation over land. The

analysis identified a collection of 16 recurrent and persistent circulation patterns in the area 10.0° –30.0°N; 120.0° –60.0° W during the MJJASO season for the period 1997–2013.

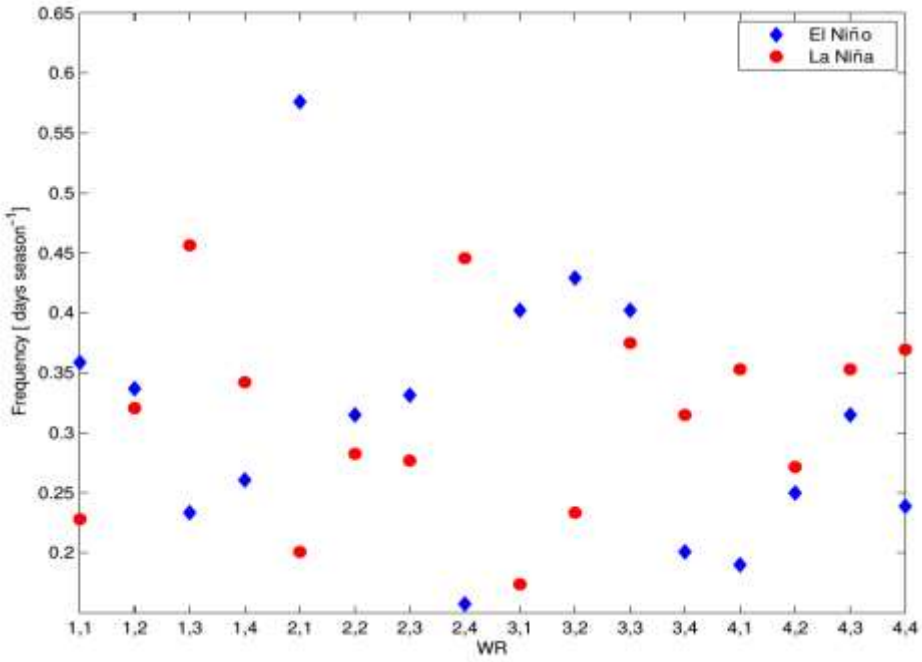


Figure 16. Relative frequency (days/season) for each weather type on 'EN' and 'LN' years.

Table 2. Coefficients of Spearman rank correlation (ρ) between MEI and regime frequencies, and the p value that test the null hypothesis of no correlation against the alternative that there is a nonzero correlation.

| WR | $\rho$ | $p$ value | WR | $\rho$ | $p$ value |
|---|---|---|---|---|---|
| 1,1 | 0.10 | 0.6947 | 3,1 | **0.58** | 0.0141 |
| 1,2 | −0.10 | 0.7146 | 3,2 | **0.63** | 0.0073 |
| 1,3 | **−0.55** | 0.0217 | 3,3 | 0.11 | 0.6656 |
| 1,4 | −0.24 | 0.3637 | 3,4 | −0.18 | 0.4878 |
| 2,1 | **0.69** | 0.0022 | 4,1 | −0.44 | 0.0767 |
| 2,2 | 0.07 | 0.7980 | 4,2 | −0.12 | 0.6354 |
| 2,3 | 0.40 | 0.1164 | 4,3 | −0.13 | 0.6181 |
| 2,4 | −0.43 | 0.0871 | 4,4 | −0.27 | 0.2979 |

If p value < 0.05, the correlation is significantly different from zero. Those coefficients are indicated in boldface.

The classification of the WRs obtained from the SOM technique allowed the identification of some of the main weather patterns that dominate in the region. Those WRs were associated with anomalous rainfall over two subregions of interest in central–southern Mexico: the Balsas River basin subregion in the west and the Yucatan subregion in the east. The analysis allowed for the discrimination of wet and dry regimes that dominate over each subregion. WRs on the top right corner of the SOM matrix represented patterns of negative MSLP anomalies, southerly vector winds, above-average low-level moisture and little influence of the NASH over southern Mexico, inducing above-normal precipitation on average. Similarly, the WRs on the bottom left corner of the SOM matrix described patterns of positive MSLP anomalies, north-easterly vector winds, below-average low-level moisture and large influence of the NASH over southern Mexico, inducing below-normal precipitation, as an average. WRs on the top right (bottom left) corner of the SOM matrix represent patterns of negative (positive) MSLP anomalies, southerly (north-easterly) vector winds, above-average (below-average) low-level moisture and little (large)

influence of the NASH over southern Mexico, inducing, above-normal (below-normal) precipitation on average.

WRs at the centre-left of the SOM grid (2,1; 2,2; 3,1; 3,2) were associated with the MSD, those occur during late July and early August, and evidence reduced low-level humidity, a strong influence of the NASH and strong easterly winds (>5 m/s, as an average), specially in the Caribbean Basin, accelerating near the Tehuantepec Isthmus and inducing below-normal rainfall all over the area. An exception is observed over the Yucatan subregion for WRs 2,2 and 3,1, which may be due to local and thermodynamic factors rather than a dominant synoptic circulation pattern.

The inter-annual variability of the rainfall associated with the WRs is well captured, the main pattern representing the MSD (2,1) has an oscillation of 3–4 years (an increase of its frequency), inducing a pattern of strong surface winds and reduced moisture in the lower troposphere and enhancing the MSD, which results in a longer and drier intra-estival drought. This WR presents about 15 more events, on average, in dry than in wet years and has a significant positive correlation (∼0.69) with the MEI, suggesting a possible modulation of its occurrence by ENSO. During EN years, the horizontal temperature gradient between the Tropical Eastern Pacific and adjacent land weakens because of the warming of the sea surface, causing a decrease in convection and a reduction of the local effect on precipitation. This fact can partially explain the negative rainfall anomalies under WR 2,1 in EN years, especially for southwestern Mexico, in particular the Balsas basin. This specific result agrees with Alfaro (2014) who found that warmer conditions in the Niño 3.4 region tend to be associated with drier MSD events in Central America. The WRs at the top right corner also appear to be modulated by ENSO phases, exhibiting negative correla tions between their frequencies and the MEI, and inducing an increase in seasonal rainfall accumulations during LN years, coinciding with an increase of their frequencies (see years 1998, 2010, 2011 and 2013 on Figure 14). Thus, ENSO could modulate the probability of occurrence of some WRs, which allows the association of EN and LN events to the prevalence of a particular regime during the summer season.

The analysis of anomalously wet and dry years for both the Balsas and Yucatan subregions suggests that year-to-year variations in the frequency of the WRs may impact the inter-annual variability of precipitation over southern Mexico, through variations in the main synoptic patterns in the lower and middle troposphere. In particular, a high-pressure anomaly centred on ∼27°N and 100°W, with anomalous anticyclonic wind flow and negative 925-hPa-specific humidity anomalies is able to weaken convection, seen in WRs located at the left bottom corner of the SOM matrix: 3,1; 4,1; 4,2. These WRs are more likely to occur in anomalously dry years. Similarly, a low-pressure anomaly centred on ∼30°N and 100°W, with anomalous cyclonic wind flow and positive 925-hPa-specific humidity anomalies is able to enhance convection, consistent with Wrs located at the right top corner of the SOM matrix: 1,3; 1,4; 2,4; which are more likely to occur in anomalously wet years.

This study highlights the importance of the large-scale tropical atmospheric circulation in the development of deep convection and rainfall over southern Mexico. Further research on this topic should incorporate other atmospheric or oceanic variables to the SOM algorithm, as well as extend the period of analysis, with the aim of exploring more thoroughly the dynamics of climatic features and their temporal variability. Furthermore, this methodology may be used to project the WRs onto regional climate model outputs, in order to assess the ability of such models to represent the dominant circulation patterns.

## Acknowledgements

The authors acknowledge the collaboration of Roberto Carlos Cruz Rodríguez and Víctor Mendoza Castro, and the comments and suggestions of the reviewers. The availability of the public data sets of ECMWF and CHIRPS was highly helpful. The authors declare no conflict of interest for this article.

## References

Alexander L, Uotila P, Nicholls N, Lynch A. 2010. A new daily pressure dataset for Australia and its application to the assessment of changes in synoptic patterns during the last century. J. Clim. 23(5): 1111–1126. https://doi.org/10.1175/2009JCLI2972.1.

Alfaro EJ. 2014. Caracterización del “veranillo” en dos cuencas de la vertiente del Pacífico de Costa Rica, América

Central. Int. J. Trop. Biol. 62(4): 1–15.
Amador J. 1998. A climatic feature of the tropical Americas: the trade wind easterly jet. Tóp. Meteorol. Oceanogr. 5(2): 91–102.
Bao M, Wallace JM. 2015. Cluster analysis of Northern Hemisphere wintertime 500-hPa flow regimes during 1920–2014. J. Atmos. Sci. 72: 3597–3608. https://doi.org/10.1175/JAS-D-15-0001.1.
Blackshear B, Crocker T, Drucker E, Filoon J, Knelman J, Skiles M. 2011. Hydropower vulnerability and climate change: a framework for modeling the future of global hydroelectric resources. In Middlebury College Environmental Studies Senior Seminar.
Brito-Castillo L, Douglas A, Leyva-Contreras A, Lluch-Belda D. 2003. The effect of large-scale circulation on precipitation and streamflow in the Gulf of California continental watershed. Int. J. Climatol. 23(7): 751–768. https://doi.org/10.1002/joc.913.
Cassano E, Lynch A, Cassano JJ, Koslow M. 2006. Classification of synoptic patterns in the western Arctic associated with extreme events at Barrow, Alaska, USA. Clim. Res. 30(2): 83–97. https://doi.org/10.3354/cr030083.
Cavazos T. 1999. Large-scale circulation anomalies conducive to extreme precipitation events and derivation of daily rainfall in northeastern Mexico and southeastern Texas. J. Clim. 12: 1506–1523.
Cavazos T. 2000. Using self-organizing maps to investigate extreme climate events: an application to wintertime precipitation in the Balkans. J. Clim. 13: 1718–1732.
Cavazos T, Comrie AC, Liverman DM. 2002. Intraseasonal variability associated with wet monsoons in southeast Arizona. J. Clim. 15: 2477–2490.
Chattopadhyay R, Sahai AK, Goswami BN. 2008. Objective identification of nonlinear convectively coupled phases of monsoon intraseasonal oscillation: implications for prediction. J. Atmos. Sci. 65(5): 1549–1569. https://doi.org/10.1175/2007JAS2474.1.
Chattopadhyay R, Vintzileos A, Zhang Z. 2013. A description of the Madden–Julian oscillation based on a self-organizing map. J. Clim. 26: 1716–1732. https://doi.org/10.1175/JCLI-D-12-00123.1.
Conde C, Ferrer R, Gay C. 1998. Variabilidad climática y agricultura. Geo UNAM 51(1): 26–32.
Conde C, Ferrer R, Orozco S. 2006. Climate change and climate variability impacts on rainfed agricultural activities and possible adaptation measures. A Mexican case study. Atmósfera 19(3): 181–194.
Curtis S. 2013. Daily precipitation distributions over the intra-Americas seas and their inter-annual variability. Atmósfera 26(2): 243–259. https://doi.org/10.1016/S0187-6236(13)71074-9.
Deligiorgi D, Philippopoulos K, Kouroupetroglou G. 2014. An assessment of self-organizing maps and k-means clustering approaches for atmospheric circulation classification. In Proceedings of the 2014 International Conference on Environmental Science and Geoscience. Paper presented at the ESG'14, Venice, Italy, 17–23.
Elghazel H, Benabdeslem K. 2014. Different aspects of clustering the self-organizing maps. Neural Process. Lett. 39(1): 97–114. https://doi.org/10.1007/s11063-013-9292-y.
Englehart P, Douglas A. 2001. The role of eastern North Pacific tropical storms in the rainfall climatology of western Mexico. Int. J. Climatol. 21: 1357–1370. https://doi.org/10.1002/joc.637.
Englehart P, Douglas A. 2006. Defining intraseasonal rainfall variability within the North American monsoon. J. Clim. 19: 4243–4253. https://doi.org/10.1175/JCLI3852.1.
Englehart P, Douglas A. 2010. Diagnosing warm-season rainfall variability in Mexico: a classification tree approach. Int. J. Climatol. 30(5): 694–704. https://doi.org/10.1002/joc.1934.
Espinoza JC, Lengaigne M, Ronchail J, Janicot S. 2012. Large-scale circulation patterns and related rainfall in the Amazon Basin: a neuronal networks approach. Clim. Dyn. 38(1): 121–140. https://doi.org/10.1007/s00382-011-1010-8.
Finnis J, Cassano JJ, Holland M, Serreze M. 2009a. Synoptically forced hydroclimatology of major Arctic watersheds in general circulation models, part 1: the Mackenzie River Basin. Int. J. Climatol. 29(9):1226–1243. https://doi.org/10.1002/joc.1753.
Finnis J, Cassano JJ, Holland M, Serreze M, Uotila P. 2009b. Synoptically forced hydroclimatology of major Arctic watersheds in general circulation models, part 2: Eurasian watersheds. Int. J. Climatol. 29(9): 1244–1261. https://doi.org/10.1002/joc.1769.
Funk C, Peterson P, Landsfeld M, Pedreros D, Verdin J, Shukla S, Husak G, Rowland J, Harrison L, Hoell A, Michaelsen J. 2015. The climate hazards infrared precipitation with stations – a new environmental record for monitoring extremes. Sci. Data 2: 150066. https://doi.org/10.1038/sdata.2015.66.

García E. 1965. Distribución de la precipitación en la República Mexicana. Publicaciones del Instituto de Geografía, UNAM, México 1, 171–191.
Guèye AK, Janicot S, Niang A, Sawadogo S, Sultan B, Diongue-Niang A, Thiria S. 2011. Weather regimes over Senegal during the summer monsoon season using self-organizing maps and hierarchical ascendant classification. Part I: synoptic time scale. Clim. Dyn. 36(1): 1–18. https://doi.org/10.1007/s00382-010-0782-6.
Gutiérrez J, Cano R, Cofino A, Sordo C. 2005. Analysis and downscaling multi-model seasonal forecasts in Peru using self-organizing maps. Tellus A 57(3): 435–447. https://doi.org/10.1111/j.1600-0870.2005 .00128.x.
Henderson GR, Barret BS, South K. 2017. Eurasian October snow water equivalent: using self-organizing maps to characterize variability and identify relationships to the MJO. Int. J. Climatol. 37(2): 596–606. https://doi.org/10.1002/joc.4725.
Hewitson B, Crane R. 2002. Self-organizing maps: applications to synoptic climatology. Clim. Res. 22(1): 13–26. https://doi.org/10.3354/cr022013.
Higgins R, Chen Y, Douglas A. 1999. Interannual variability of the North American warm season precipitation regime. J. Clim. 12(3): 653–680.
Hope P. 2006. Projected future changes in synoptic systems influencing southwest Western Australia. Clim. Dyn. 26(7): 765–780. https://doi.org/10.1007/s00382-006-0116-x.
Huffman G, Bolvin D. 2013. Version 1.2 GPCP one-degree daily precipitation data set documentation. Mesoscale Atmospheric Processes Laboratory, NASA Goddard Space Flight Center and Science Systems and Applications, Inc, 27 pp. http://apdrc.soest.hawaii.edu/doc/gpcp_daily.pdf (accessed 2 June 2017).
Johnson NC, Feldstein SB. 2010. The continuum of North Pacificsea level pressure patterns: intraseasonal, interannual, and interdecadal variability. J. Clim. 23: 851–867. https://doi.org/10.1175/2009JCLI3099.1.
Johnson NC, Feldstein SB, Tremblay B. 2008. The continuum of Northern Hemisphere teleconnection patterns and a description of the NAO shift with the use of self-organizing maps. J. Clim. 21: 6354–6371.https://doi.org/10.1175/2008JCLI2380.1.
Karnauskas K, Seager R, Giannini A, Busalacchi A. 2013. A simple mechanism for the climatological mid-summer drought along the Pacific coast of Central America. Atmósfera 26(2): 261–281. https://doi.org/10.1016/S0187-6236(13)71075-0.
Kimoto M, Ghil M. 1993. Multiple flow regimes in the Northern Hemisphere winter. Part II: sectorial regimes and preferred transitions. J. Atmos. Sci. 50(16): 2645–2673.
Kohonen T. 1982. Self-organized formation of topologically correct feature maps. Biol. Cybern. 43(1): 59–69. https://doi.org/10.1007/BF00337288.
Kohonen T. 2001. Self-Organizing Maps, 3rd edn. Springer-Verlag: New York, NY.
Kondrashov D, Ide K, Ghil M. 2004. Weather regimes and preferred transition paths in a three-level quasi-geostrophic model. J. Atmos. Sci. 61(5): 568–587.
Liebmann B, Bladé I, Bond N, Gochis D, Allured D, Bates GT. 2008. Characteristics of North American summertime rainfall with emphasis on the monsoon. J. Clim. 21: 1277–1294. https://doi.org/10.1175/2007JCLI1762.1.
Liverman D. 1990. Drought impacts in Mexico: climate, agriculture, technology, and land tenure in Sonora and Puebla. Ann. Assoc. Am. Geogr. 80(1): 49–72. https://doi.org/10.1111/j.1467-8306.1990.tb00003.x.
MacKellar N, Tadross M, Hewitson B. 2010. Synoptic-based evaluation of climatic response to vegetation change over southern Africa. Int. J. Climatol. 30(5): 774–789. https://doi.org/10.1002/joc.1925.
MacQueen J. 1967. Some methods for classification and analysis of multivariate observations. In Berkeley Symposium on Mathematical Statistics and Probability, University of California Press, 281–297.
Magaña V, Caetano E. 2005. Temporal evolution of summer convective activity over the Americas warm pools. Geophys. Res. Lett. 32(2): L02803. https://doi.org/10.1029/2004GL021033.
Magaña V, Amador J, Medina S. 1999. The midsummer drought over Mexico and Central America. J. Clim. 12: 1577–1588.
Magaña V, Vázquez J, Pérez J, Pérez J. 2003. Impact of El Niño on precipitation in Mexico. Geofís. Int. 42(3): 313–330.
Méndez M, Magaña V. 2010. Regional aspects of prolonged meteorological droughts over Mexico and Central America. J. Clim. 23: 1175–1188.
Mendoza V, Oda B, Garduño R, Villanueva E, Adem J. 2014. Simulation of the PDO effect on the North America summer climate with emphasis on Mexico. Atmos. Res. 137: 228–244.

https://doi.org/10.1016/j.atmosres.2013.10.010.
Nishiyama K, Endo S, Jinno K, Uvo CB, Olsson J, Berndtsson R. 2007. Identification of typical synoptic patterns causing heavy rainfall in the rainy season in Japan by a self-organizing map. Atmos. Res. 83(2–4):185–200. https://doi.org/10.1016/j.atmosres.2005.10.015.
Oettli P, Tozuka T, Izumo T, Engelbrecht FA, Yamagata T. 2014. The self-organizing map, a new approach to apprehend the Madden–Julian Oscillation influence on the intraseasonal variability of rainfall in the southern African region. Clim. Dyn. 43(5): 1557–1573. https://doi.org/10.1007/s00382-013-1985-4.
Ohba M, Kadokura S, Yoshida Y, Nohara D, Toyoda Y. 2015. Anomalous weather patterns in relation to heavy precipitation events in Japan during the Baiu Season. J. Hydrometeorol. 16(2): 688–701. https://doi.org/10.1175/JHM-D-14-0124.1.
Polo I, Ullmann A, Roucou P, Fontaine B. 2011. Weather regimes in the Euro-Atlantic and Mediterranean sector and relationship with West African rainfall over the period 1989–2008 from a self-organizing maps approach. J. Clim. 24(13): 3423–3432. https://doi.org/10.1175/2011JCLI3622.1.
Reusch D, Alley R, Hewitson B. 2007. North Atlantic climate variability from a self-organizing map perspective. J. Geophys. Res. 112:D02104. https://doi.org/10.1029/2006JD007460.
Romero-Centeno R, Zavala-Hidalgo J, Raga G. 2007. Midsummer gap winds and low-level circulation over the eastern tropical Pacific.J. Clim. 20: 3768–3784. https://doi.org/10.1175/JCLI4220.1.
Sáenz F, Durán-Quesada AM. 2015. A climatology of low level wind regimes over Central America using a weather type classification approach. Front. Earth Sci. 3(15): 1–18. https://doi.org/10.3389/feart.2015.00015.
Sheridan SC, Lee CC. 2011. The self-organizing map in synoptic climatological research. Prog. Phys. Geogr. 35(1): 109–119. https://doi.org/10.1177/0309133310397582.
Skific N, Francis JA, Cassano JJ. 2009a. Attribution of projected changes in atmospheric moisture transport in the Arctic: a self-organizing map perspective. J. Clim. 22: 4135–4153. https://doi.org/10.1175/2009JCLI2645.1.
Skific N, Francis JA, Cassano JJ. 2009b. Attribution of seasonal and regional changes in Arctic moisture convergence. J. Clim. 22:5115–5134. https://doi.org/10.1175/2009JCLI2829.1.
Steynor A, Hewitson B, Tadross M. 2009. Projected future runoff of the Breede River under climate change. Water SA 35(4): 433–440.
Tennant W, Hewitson B. 2002. Intra-seasonal rainfall characteristics and their importance to the seasonal prediction problem. Int. J. Climatol. 22(9): 1033–1048. https://doi.org/10.1002/joc.778.
Tozuka T, Luo J, Masson S, Yamagata T. 2008. Tropical Indian Ocean variability revealed by self-organizing maps. Clim. Dyn. 31(2):333–343. https://doi.org/10.1007/s00382-007-0356-4.
Tymvios F, Savvidou K, Michaelides S. 2010. Association of geopotential height patterns with heavy rainfall events in Cyprus. Adv. Geosci. 23: 73–78. https://doi.org/10.5194/adgeo-23-73-2010.
Vautard R, Mo KC, Ghil M. 1990. Statistical significance test for transition matrices of atmospheric Markov chains. J. Atmos. Sci. 47(15): 1926–1931.
Vázquez-Aguirre JL. 2007. Variabilidad de la precipitación en la República Mexicana (Variability of Precipitation in Mexican Republic). Masters thesis, Universidad Nacional Autónoma de México, Ciudad Universitaria, México.
Vesanto J, Alhoniemi E. 2000. Clustering of the self-organizing map. IEEE Trans. Neural Netw. 11(3): 586–600. https://doi.org/10.1109/72.846731.
Vesanto J, Himberg J, Alhoniemi E, Parhankangas J. 2000. SOM Toolbox for Matlab 5. Helsinki University of Technology: Finland. http://www.cis.hut.fi/projects/somtoolbox/package/papers/techrep.pdf (accessed 10 June 2016).
Wang C. 2007. Variability of the Caribbean low-level jet and its relations to climate. Clim. Dyn. 29(4): 411–422. https://doi.org/10.1007/s00382-007-0243-z.
Wolter K, Timlin M. 1993. Monitoring ENSO in COADS with a seasonally adjusted principal component index. In Proceedings of the 17th Climate Diagnostics Workshop, Norman, OK, 52–57.